# Nanoscale Investigation into Dynamics of Thin Liquid Films During Bouncing and Attachment of Rising Air Bubbles on Hydrophilic and Hydrophobic Surfaces

by

Fatemeh Hamidzadeh<sup>1</sup>, Kaiwu Huang<sup>1</sup>, Xinyu Ye<sup>2</sup>, and Lei Pan<sup>1,\*</sup>

- Department of Chemical Engineering, Michigan Technological University, 1400 Townsend Drive, Houghton, MI 49931
- 2. Department of Civil, Environmental and Geospatial Engineering, Michigan Technological University, 1400 Townsend Drive, Houghton, MI 49931

#### **Abstract**

Bouncing and attachment of free-rising air bubbles on hydrophobic surfaces has been limited to side-view, high-speed photography of the bubble-plate attachment process. In this work, an investigation on the dynamics as well as stability of thin liquid films (TLFs) between free-rising air bubbles and quartz surfaces was performed using a newly developed multiple-wavelength synchronized reflection interferometry microscopy (SRIM) technique. The effect of surface hydrophobicity on both the stability and critical rupture thickness of TLFs was investigated. Results showed that the TLF ruptured at a critical rupture thickness of 100-1000 nm or beyond during a bubble's impact on hydrophobic surfaces. The critical rupture thicknesses varied depending on surface hydrophobicity as well as surface asperity. A higher surface hydrophobicity in general contributed to a higher critical rupture thickness. In addition, the effect of n-octanol on the stability of TLFs was investigated. Results showed that film stability increased with increasing the concentration of n-octanol, which was accompanied with a significant decrease in the critical rupture thickness. The present result illustrates, for the first time, the dynamics of TLFs on hydrophobic surfaces under a dynamic condition compared with previous studies under a quasi-equilibrium condition. The information revealed from the present work has a significant implication to many industrial applications including froth flotation and other biological and semiconductor applications.

#### \*Corresponding author

Email: <u>leipan@mtu.edu</u>

Phone: (906) 487-2569

#### 1. Introduction

Thin liquid films (TLFs) are formed when two surfaces are sandwiching a liquid medium in between. Foam film typically refers to a TLF sandwiched by two air bubbles, while the wetting film refers to a TLF sandwiched by one air bubble and one solid surface. The stability of the TLFs is essential to many applications, including froth flotation process<sup>1-3</sup>, foam film<sup>4</sup>, and bitumen oil recovery<sup>5, 6</sup>. A stable thin liquid film (TLF) may be favorable in some applications, while in many other applications an unstable TLF is more desirable. Thermodynamically, the stability of TLFs is governed by the changes in the Gibbs free energy ( $\Delta$ G) associated with the film rupture. For instance, foam film in deionized (DI) water is thermodynamically unstable with  $\Delta$ G = - 142 mN/m.

Past efforts have been made to investigate the stability of thin liquid film (TLFs) between two surfaces. This was accomplished by bringing the two surfaces close to each other in a liquid medium<sup>7, 8</sup> or by withdrawing liquid between the two interfaces<sup>9</sup>. Past research was carried out at a low Reynolds number condition, at which the fluid velocity within the TLFs was typically in the range of 0-100 µm/s. The reflection interferometry microscopy (RIM) technique using a monochromatic light source has been employed to determine the thickness of the TLFs. On a hydrophilic quartz surface, a stable wetting film was formed due to the presence of a repulsive disjoining pressure that balances the capillary pressure. For unstable TLFs, the TLFs ruptured at 0-200 nm<sup>10-12</sup>. These experiments were carried out between two air bubbles in water<sup>12</sup>, between one air bubble and one hydrophobic surface<sup>11</sup>, and between one oil droplet and one hydrophobic solid surface<sup>10</sup>. The drainage of TLFs has been successfully modelled by the Reynolds lubrication theory coupled with the DLVO theory<sup>11, 13</sup>. All models assume a non-slip boundary condition at the air/water and solid/water interfaces. Results obtained from numerical modelling matched well with the experimental data, confirming a non-slip boundary condition at the two interfaces<sup>14</sup>.

Despite the fact that the modeling on film drainage has been well studied, the mechanism on film rupture of the TLFs is still elusive. The mechanism for the film rupture has been investigated and reviewed<sup>15</sup>. Various theories have been proposed, including 1) nanobubble theory<sup>16, 17</sup>, 2) hydrophobic disjoining pressure<sup>11, 13</sup>, 3) gas cavity<sup>18</sup>, and 4) wave theory<sup>19</sup>. It has been claimed that the film rupture for wetting films formed on hydrophobic surfaces was a result of rupture of the foam films locally formed between the colliding macro-bubble and nano- and/or sub-microscopic bubbles already attached to the hydrophobic surfaces<sup>20</sup>. However, this theory has not been directly confirmed due to the experimental limitation in detecting nanobubbles on solid surfaces during the bubble-solid attachment. In addition, both short-range and long-range hydrophobic forces have been claimed to be the driving forces for the film rupture<sup>10, 11</sup>. However, the effective range for this attractive hydrophobic force has not been settled, and the effective range varies depending on surface treatment method<sup>21</sup>, solution chemistry<sup>22</sup>, electric charges on surfaces<sup>23</sup>, and temperature<sup>24</sup>.

Recent studies have been extended to both experimental studies and theoretical modelling on the impact of free-rising air bubbles on both hydrophilic and hydrophobic flat surfaces. Under these conditions, the impact velocity of the air bubble can be as high as 1000 mm/s, at which its approaching velocity is several orders higher than the experimental condition used in studying film stability and film drainage as described earlier<sup>25</sup>. These experimental studies relies on high-speed cameras to capture fast-evolving bubbles during their impact with the upper quartz plates<sup>26</sup>. During the impact of the air bubble on a flat solid surface, the air bubble bounces on and off the surface multiple times<sup>26, 27</sup>. On a very hydrophilic

surface, the air bubble stays against the flat surface with a stable TLF trapped in between. On the hydrophobic surface, the air bubble readily spreads on the hydrophobic solid surface after a few bounces on the surfaces<sup>28</sup>. It has been previously documented that both the surface roughness<sup>29</sup> and surfactants in aqueous solutions<sup>20</sup> impact the lifetime of film drainage. For instance, the time for the film drainage in DI water was in the order of 20 ms for both hydrophobic Teflon 2500 and silanized glass surfaces. When  $10^{-3}$  M n-octanol was added to the water, the time for film drainage was significantly increased, to approximately 100 ms. This result suggested that the film drainage was de-accelerated in the presence of n-octanol in the aqueous solutions. It is unclear whether the reduced kinetics of film drainage could be attributed to an increase in critical rupture thickness.

Recent efforts have been made to study the dynamics of thin liquid films (TLFs) formed between free-rising air bubbles and rigid solid surfaces<sup>30</sup>. Direct monitoring of the thickness profiles during the bouncing and impact of free-rising air bubbles and flat hydrophilic plates has been made possible recently<sup>30-32</sup>. The film thickness of the TLF was directly observed using the interferometry technique. Parkinson and Ralston monitored the drainage of TLFs when a tiny air bubble was rising against a flat surface<sup>32</sup>, and the experimental data was compared with the modelling results using a force balance coupled with colloidal forces or DLVO forces<sup>33</sup>. However, little information on the dynamics of wetting films formed on hydrophobic surfaces was available due to the technical challenges of tracking the dynamics of unstable TLFs on hydrophobic surfaces. The mechanism of the rupture of TLFs under industrial-relevant froth flotation conditions, *i.e.*, the impact of a free-rising air bubble and a solid surface, was still elusive.

In this work, the stability of TLFs during the impact of free rising air bubbles on flat hydrophilic and hydrophobic plates was investigated using two-wavelength synchronized reflection interferometry microscopy (SRIM). The bubbles' impacting velocity was in the range of 200-800 mm/s. The air bubbles bounced on the flat surfaces, with the maximum bounce-off distance decreasing after each bounce. The quartz surfaces were rendered hydrophobic through a silanization reaction and the use of cationic surfactants. A spatiotemporal thickness profile of the wetting films was determined from the recorded interference fringes. From the spatiotemporal thickness profile, the critical rupture thickness of the wetting films was determined. In addition, the effect of surface-active chemicals on the stability of TLFs was investigated. The critical rupture thickness and lifetime results were discussed in the context of literature data on the critical rupture thickness of wetting films obtained in quasi-equilibrium conditions.

# 2. Materials and Experiments

#### 2.1 Materials

Polished fused quartz plates (1" x 1" x 0.062") were obtained from Technical Glass Products (TGP). The root mean square (RMS) roughness of the quartz plates was 1 nm or below. The deionized (DI) water was supplied from a laboratory Barnstead water purification system (thermos fisher), and the DI water had a resistance of 18.1 m $\Omega$ .cm or above. The quartz plates were cleaned in a freshly prepared piranha solution (a mixture of sulfuric acid to hydrogen peroxide in a ratio of 7:3) at a temperature of 85 °C for 20 min. The cleaned quartz plates were rinsed with excessive amounts of DI water to remove any acid residue on surfaces and dried with an ultrapure nitrogen gas stream. The obtained quartz plates were free of contaminants. They were hydrophilic and could be wetted by DI water completely.

The quartz plates were rendered hydrophobic by a silanization reaction. Both methyltrichlorosilane (MTS) and trichloro-octadecylsilane (OTS) chemicals were used, having been obtained from Sigma Aldrich and TCI America. The hydrophobization process involves an immersion of dry quartz plates in OTS-in-toluene or MTS-in-toluene solutions. The surface hydrophobicity of the hydrophobic quartz plates was controlled by the concentration of silane chemicals and reaction time. The concentration of OTS/OTS in the toluene solutions was  $10^{-3}$  M to  $10^{-2}$  M. The surface hydrophobicity of the quartz plates was determined by a contact angle goniometer using the sessile drop technique. Contact angle measurements were conducted at least 5 times, and average data was reported. In addition, the quartz plates were hydrophobized by immersing freshly cleaned quartz plates in  $10^{-4}$  M cetyltrimethylammonium bromide (CTAB) aqueous solution for 10-30 minutes. The water contact angle of the hydrophobized quartz plates was determined by the captive bubble method.

#### 2.2 Experimental Configuration

#### 2.2.1 Physical Configuration

The stability of thin liquid films (TLFs) or wetting films formed between a rising air bubble and a hydrophobic quartz plate was investigated using a customized experimental configuration. Figure 1 shows a schematic drawing of an experimental setup which was developed to study the microscopic dynamics of thin liquid films (TLF). A square glass container ( $20 \times 20 \times 25$  cm) was custom fabricated and filled with DI water. A transparent quartz plate was attached onto a cage plate (Thorlabs) by vacuum grease, which allowed light to pass through the quartz plate. A 26-gauge stainless-steel needle (OD = 0.464 mm and ID = 0.260 mm, Hamilton, NV) was used to generate one single air bubble. The needle was carefully bent with its tip at 5-10 cm away from the upper quartz plate. A custom manual screw syringe pump was fabricated and used to create one air bubble with a diameter of 0.5-2.5 mm. The size of the air bubble was controlled by the size of the needle tip and its surface hydrophobicity. The air bubble was released from the tip and rose freely against the upper quartz plate.

#### 2.2.2 Optical Systems

The experimental configuration consists of two major instrumentations, including a) a side-view, high-speed camera monitoring bubble dynamics and b) a synchronized reflection interferometry microscope (SRIM) monitoring dynamics of thin liquid film (TLFs) formed during the bubbles' impact on the solid surface. A high-speed camera (AX200, Photron) with an adjustable 50-mm lens and a lighting system was used to capture the bubbles' impact and bounce on flat quartz plates. This high-speed camera captures the bubble's dynamics at 6400 frames per second. The side-view images were analyzed using TRACKER software to determine the trajectory and velocity of the air bubble.

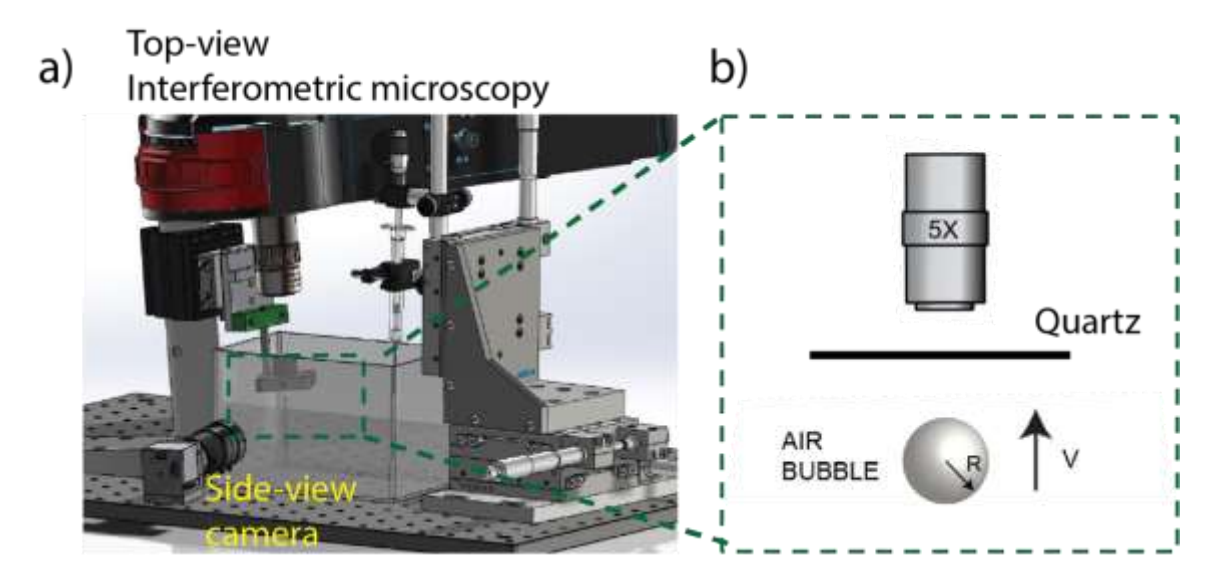


Figure 1. A schematic of an experimental configuration to study the collision and impact of a free-rising air bubble on a stationary horizontal solid surface: (a) a 3D drawing of the experimental configuration and b) a zoom-in view of a thin liquid film (TLF) confined between a fixed solid plate and a free-rising air bubble.

During a bubble's impact on a solid plate, a thin liquid film (TLF) was formed between a rising air bubble and a stationary quartz plate. The spatial and temporal evolution of the thickness profiles of TLFs was investigated using the reflection interferometry microscopy (RIM) technique. In this work, a two-wavelength synchronized reflection interferometry microscope coupled with two cameras was employed to capture fast-evolving interference fringes simultaneously at two distinct wavelengths (460 and 526 nm). An upright microscope system with a 5X ultra-long working distance objective (Mitutoyo) was used to monitor the interference fringes of wetting films. The depth of the focus with this 5x ultralong working distance objective was 2.4  $\mu$ m. Out of this thickness range, the interference fringe became blurry and unviable.

Figure 2 shows an optical configuration of the two-wavelength synchronized reflection interferometric microscopy (SRIM) system. Two high-power monochromatic LEDs were used to generate incident light beams. The two incident light beams were combined by a dichroic mirror. In this study, two synchronized CMOS cameras (Grasshopper3, FLIR) recorded the interference fringes simultaneously at a rate of 250 fps. Short-pass filters with a full width at half maximum (FWHM) of 10 nm were installed at the front of two individual cameras to create a monochromatic interference fringe nm at central wavelengths of 460 nm and 526 nm, respectively. The focus of the two cameras was adjusted when the needle was placed exactly at the center of the objective lens with an air bubble attached to it. The focus was adjusted by manually moving the needle towards the plate until the interference fringe became visible. Two cameras were synchronized using an onboard hardware and a trigger system. The capture rate of the two CMOS cameras was controlled by a function generator (Tektronix). The recording started after an air bubble was released. In this study, the range for the accurate film thickness measurement was 0-1000 nm, with a maximum detection limit of 2.4 um. The starting time was reset at the point when the air bubble first hit the quartz plate.

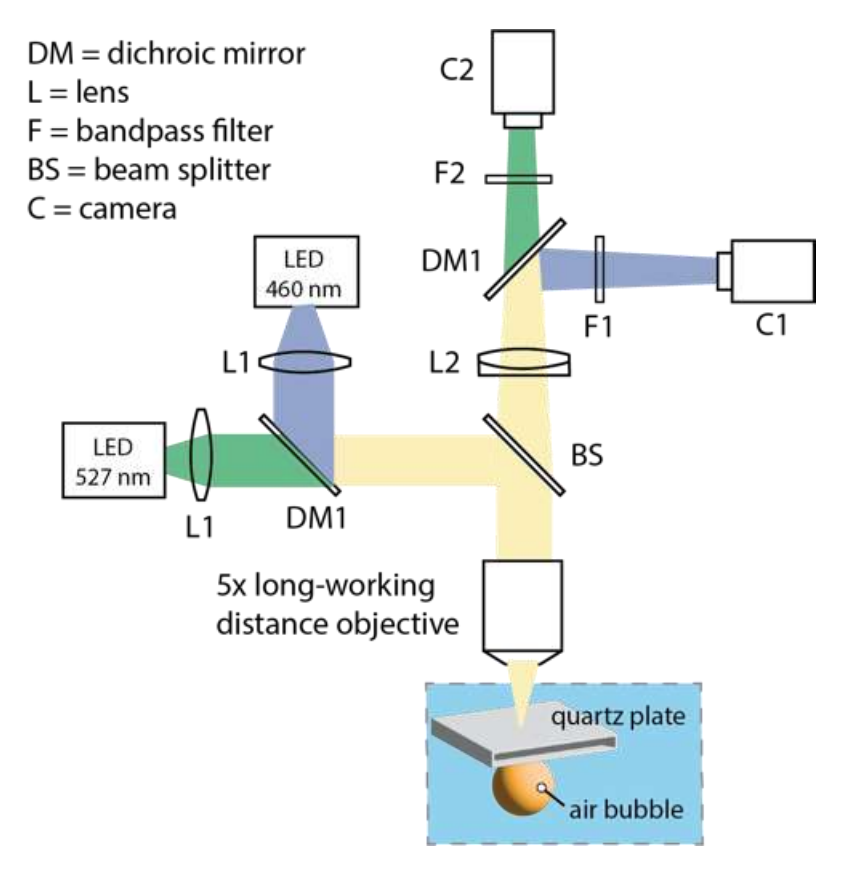


Figure 2. An optical configuration of a multi-wavelength synchronized reflection interferometry microscope (SRIM).

The principle of reflection interferometry microscopy (RIM) is based on an overlap of the two reflected lights from the adjoining interfaces of the thin liquid films (TLFs). When an incident light beam hit the interfaces, the beams were reflected at two adjacent interfaces of the TLFs, creating an interference fringe. The bright fringe refers to a scenario where the two reflected light beams have the exact same phase with each other, resulting in a constructive interference fringe. In this scenario, the thickness of the TLF is equivalent to even orders of  $\lambda/4n$ , where  $\lambda$  is the wavelength of the incident light and n is the reflective index of the liquid medium. When the two reflected lights from the adjacent interfaces of the TLFs exhibit a 180-degree difference in phases with each other, an overlap of two reflected light beams causes a destructive pattern. In this scenario, the film thickness is equivalent to odd orders of  $\lambda/4n$ .

Therefore, the intensity profile of the interference pattern is given as<sup>44</sup>

$$I = I_1 + I_2 + 2\sqrt{I_1 I_2} \cos(\frac{4\pi nh}{\lambda} + \delta)$$
(1)

where  $I_1$  and  $I_2$  are the intensities of light waves reflected from two adjoining interfaces of the thin liquid films (TLFs). In Eq. (1), the optical path length (2*nh*) is a product of twice the film thickness (*h*) and the reflective index (*n*) of the medium in which the light propagates,  $\lambda$  is the light wavelength, and  $\delta$  is the phase shift of the light reflected from the interfaces. The  $\delta$  value is determined from the reflective indexes

(n, k) of the media using a matrix of a multilayer system.<sup>50</sup> Herein,  $\delta = 0$  in the thin liquid films formed between an air bubble and a quartz surface.

The interference fringes of TLFs between a hemispherical air bubble and a flat quartz plate exhibits a concentric interference fringe, which is known as Newton's rings. The Newton's rings consist of concentrically alternating bright and dark rings. From the fringes,  $I_{\text{max}}$  and  $I_{\text{min}}$  values are the maximum and minimum intensities in each adjacent pattern when the phase differences  $(4\pi nh/\lambda + \delta)$  are even and odd multiples of  $\pi$ , respectively. The film thickness at the maximum  $(I_{\text{max}})$  and minimum  $(I_{\text{min}})$  intensities are the even and odd multiples of  $\lambda/4n$ , respectively. Eq. (1) might be modified as

$$\frac{2I - (I_{\text{max}} + I_{\text{min}})}{I_{\text{max}} - I_{\text{min}}} = \cos(\frac{4\pi nh}{\lambda} + \delta)$$
 (2)

From Eq. (2), h can be determined if  $I_{\text{max}}$ ,  $I_{\text{min}}$  and n are known. Both  $I_{\text{max}}$  and  $I_{\text{min}}$  can be determined from one interference fringe image or a sequence of interference fringes.

One major challenge associated with an analysis of monochromatic interference fringes is a determination of fringe order (n) for each fringe pattern. This is particularly challenging if no reference points are identified. Alternatively, the multi-wavelength synchronized reflection interferometry microscopy (SRIM) technique uses multiple synchronized high-speed cameras to capture the monochromatic interference fringes at multiple wavelengths simultaneously. Since the interference pattern varies with the wavelengths of the incident light, the interference fringes of the TLFs exhibit distinct patterns depending on the wavelength of the incident light. By analyzing the interference fringes captured at different wavelengths, the fringe orders can be determined, as well as the thickness profile.

Image processing of the interference fringes was performed using a customized Matlab code based on the principle of interferometry, as described above. The details can be found in the Appendix. In this work, the spatial film thickness profile from a given interference fringe pattern was determined. By matching spatial film thickness profiles of thin liquid films (TLFs) obtained from two monochromatic interference fringes at two distinct wavelengths, one can accurately determine both the order of fringes and the film thickness profile with high accuracy.

#### 3. Results and Discussion

#### 3.1 Bubbles' Bouncing

Figure 3 shows side-view images of the bubbles' impact on a hydrophilic surface at two distinct release distances. Two cases are compared, including a) a short release distance (1.5 mm away from the upper quartz plate) and 2) a medium release distance (9.5 mm away from the upper quartz plate). The former case represents a low impact velocity, while the latter case represents a high impact velocity. The air bubble formed a pancake shape during its impact on a flat solid surface. A restoration of the bubble's deformation resulted in a bounce of the air bubble off the solid surface. The energy loss associated with the film drainage resulted in a reduction in the bubble's bouncing velocity, as reflected by the maximum bouncing distance after each bounce.

Figures 3c and 3d show the position of the center of the air bubble in two cases (i.e., short release distance vs. long release distance). The air bubble rose freely and impacted the upper quartz surface. The initial

impact velocities at 1.5-mm and 9.50-mm release distances were estimated to be 340 and 842 mm/s, respectively. After a few bounces off the surface, the impact velocity of the air bubble dropped to 10-25 mm/s. The kinetic energy of the air bubble was dissipated, resulting in a significant reduction in the impact velocity. The air bubble was relatively stationary against the hydrophilic quartz plate after the initial impact. On the hydrophilic quartz surface, the air bubble beaded up against the solid surface while maintaining its spherical shape.

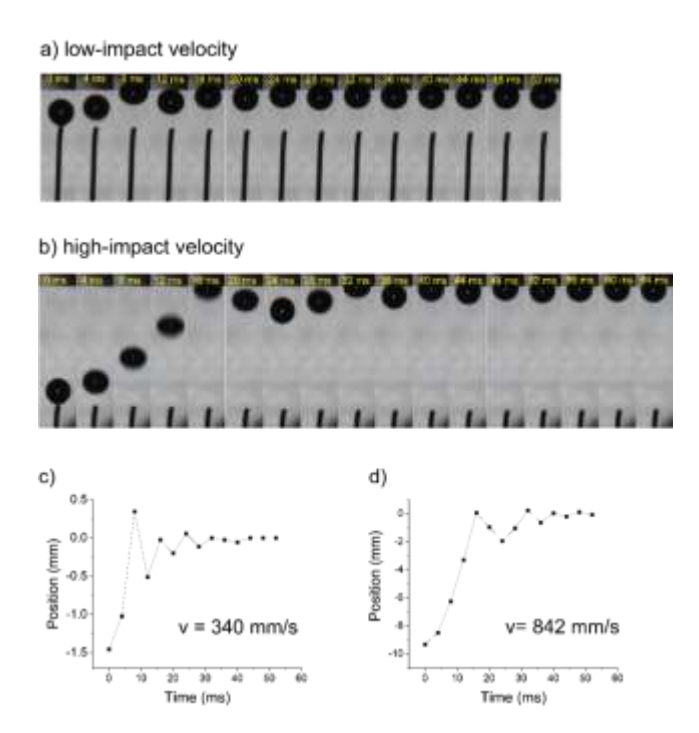


Figure 3. a) a sequence of side-view images of a free-rising air bubble of 1-mm in diameter against a hydrophilic quartz plate at 1.5-mm away from the upper quartz plate, b) a sequence of side-view images of a free-rising air bubble of 1-mm diameter against a hydrophilic quartz plate at a distance of 10 mm from the upper quartz plate, c) a tracking of the position of the center of the air bubble along the y-axis. The maximum impact velocity of the air bubble was estimated to be 340 mm/s, and d) a tracking of the position of the center of the air bubble along the y-axis.

### 3.2 Drainage of Thin Liquid Film (TLFs) on Hydrophilic Surfaces

During an impact of a free-rising air bubble against a flat quartz surface, a thin liquid film (TLF) was formed. Figure 4a shows interference fringes of the TLFs during a bubble's impact on a freshly cleaned hydrophilic quartz surface. As shown, a dimple with its minimum film thickness at the edge was initially formed at a distance far away from the plate. The dimple formation was due to a strong hydrodynamic force associated with the initial high impact velocity of the air bubble. The air bubble continued to rise against the quartz plate accompanied by a drainage of the thin liquid film. Figure 4b shows spatiotemporal thickness profiles of the TLFs as well as the error between the experimental data and polynomial fitted profiles. The spatial profiles obtained from two colored fringes ( $\lambda$  = 460 and 526 nm) matched with each

other, validating the spatial thickness measurement protocol. The peak-to-valley error was found to be less than 100 nm, with an RMS of 10 nm or below.

When the air bubble continued to rise freely against a hydrophilic quartz plate by its buoyance force, the thin liquid film (TLF) drain was followed by a flattening of the TLF on a hydrophilic quartz surface. The TLFs eventually reached an equilibrium at an equilibrium film thickness of 90-100 nm. At this equilibrium thickness, the disjoining pressure predominantly arising due to the electrostatic double layer force was balancing the capillary pressure ( $2\gamma/R$ ), where R was the radius of the air bubble. In this work, the size of the air bubble is 1.5 mm, and therefore the capillary pressure is 96 Pa. The equilibrium film thickness ( $h_e$ ) of the TLFs matches well with the literature data<sup>34</sup>.

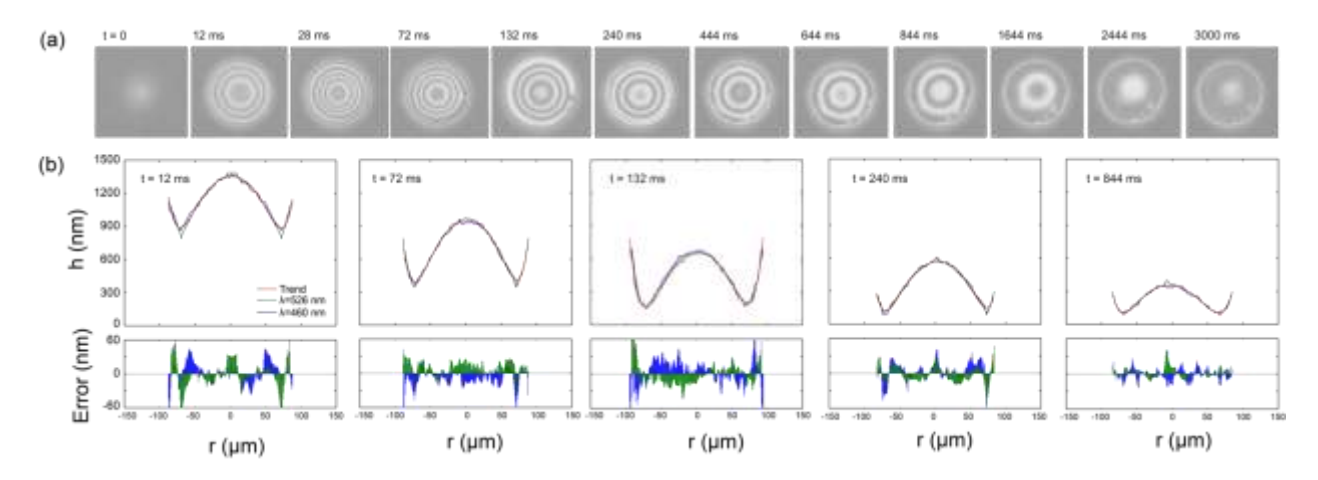


Figure 4. a) timed series of interference fringes of the thin liquid film (TLF) during an impact of a free-rising air bubble against a hydrophilic quartz plate, b) spatial thickness profiles of the TLFs across the axial-symmetric center of the fringe as a function of time obtained at  $\lambda$  = 460 nm and 526 nm, respectively. The smooth line is a polynomial fit to the experimental data. The difference between the fitted profile and the experimental data is also shown with an RMS value of less than 10 nm.

#### 3.3 Drainage of Thin Liquid Film (TLFs) on Hydrophobic Surfaces

The effect of surface hydrophobicity on the stability of TLFs formed between free-rising air bubbles and the hydrophobic quartz plates was also investigated. Figure 5a shows a sequence of the interference fringes of thin liquid films (TLFs) during an impact of air bubbles against an MTS-treated hydrophobic quartz surface. The equilibrium water contact angle of the hydrophobized quartz plate was 75°, measured by the sessile drop technique method. As shown, the initial spatial thickness profiles of the TLFs were identical to those obtained with hydrophilic quartz plates. A dimple was initially formed due to a strong hydrodynamic force associated with the bubble's impact. When the air bubble continued to push against the hydrophobic surface, the film ruptured catastrophically. The time spent from the initial impact (t = 0 ms) to the film rupture was only 20 ms. Figure 5b shows a timed series of spatial thickness profiles of the thin liquid films (TLFs) on a hydrophobic surface as well as the error between the experimental data and polynomial fitted curve. As shown, the TLF ruptured at approximately 690 nm. Once the thin liquid film

ruptured and an air channel connected both the air bubble and the hydrophobic quartz plate, a three-phase contact line (TPCL) rapidly expanded until an equilibrated contact line was established.

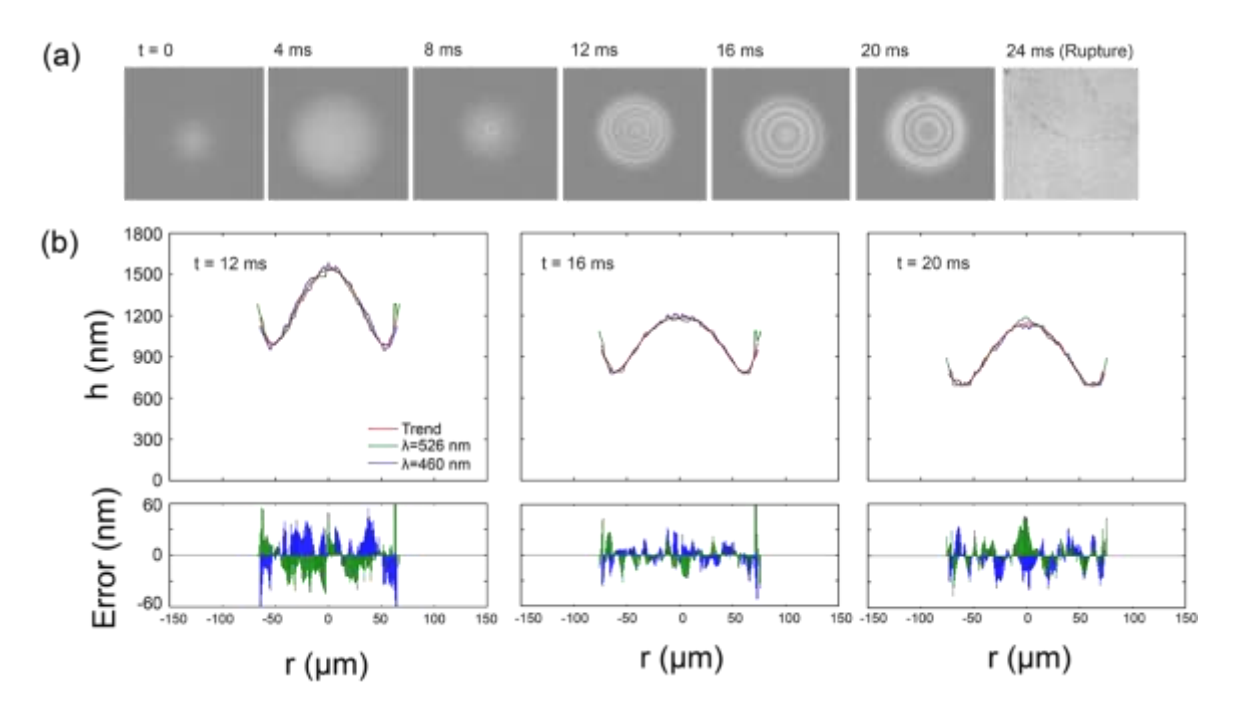
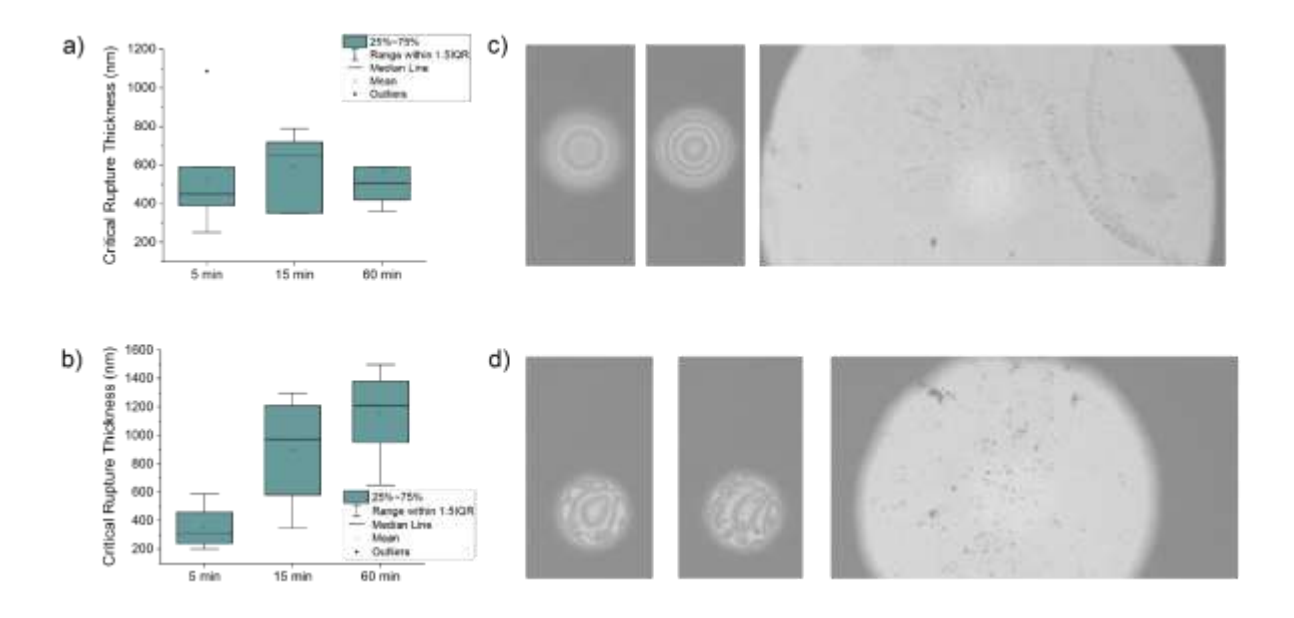


Figure 5. a) timed series of interference fringes of the thin liquid film (TLF) during an impact of a free-rising air bubble against a hydrophobic quartz plate; b) spatial thickness profiles of the TLFs across the axial-symmetric center of the fringe as a function of time obtained at  $\lambda$  = 460 nm and 526 nm, respectively. After 20 ms of an initial bubble-plate impact, the thin liquid film (TLF) ruptured. The film ruptured at approximately 690 nm.

The rupture of the TLFs was a random process, and many factors impact the film rupture process. These factors include surface hydrophobicity, surface asperity, and surface roughness. In this work, repetitive experiments were conducted to better understand the effect of surface hydrophobization on film stability and critical rupture thickness. The longer the critical rupture thickness, the shorter the film lifetime. Figure 6a shows the statistics of critical rupture thickness of TLFs on OTS-hydrophobized quartz plates. The surface hydrophobicity of the hydrophobized quartz plates increased with increasing reaction times, reaching a maximum of 95-100°. The water contact angles of the OTS hydrophobized quartz plates after 5-min, 15-min, and 60-min reaction times of silanization processes were 65°, 90°, and 95°, respectively. The medium critical rupture thicknesses of the TLFs were increased from 450 nm on OTS-treated hydrophobic surfaces with water contact angles of 65° to 580 nm on hydrophobic surfaces having 90°-95° water contact angles. There were a few scenarios at which the critical rupture thickness was above 2000 nm and the interference fringes were barely visible.

Figure 6b shows the statistics on the critical rupture thickness of wetting films formed on MTS-treated hydrophobic quartz surfaces. The MTS coating rendered the quartz plate less hydrophobic compared with the OTS coating. The water contact angles of MTS-coated surfaces were 50°, 80°, and 85° after 5, 15, and

60 minutes of the silanization process. The medium critical rupture thickness of the hydrophobic quartz plates after 5 minutes of the silanization process was approximately 300 nm. Compared with the OTS coating, the higher surface hydrophobicity facilitated the rupture of wetting films on hydrophobic surfaces. It is interesting to note that after 15 minutes and 60 minutes of silanization process with MTS, the medium critical rupture thickness of the wetting films jumped to 800-1000 nm, despite the fact that the water contact angles on these MTS-treated hydrophobic surfaces were in the range of 80-85°. There were additional factor(s) contributing to the film rupture. To better understand the rupture mechanisms involved, the moment when the film rupture occurred was closely investigated. Figure 6c and 6d shows a sequence of interference fringes right before and right after the film ruptures on OTS-treated and MTS-treated quartz plates. On the MTS-treated hydrophobic quartz plates, the surface was found to be covered with micron-sized MTS-polymerized substances, in contrast with the OTS-treated hydrophobic quartz plates. Based on the interference fringe data, it is reasonable to attribute the film rupture to the surface asperity on hydrophobic surfaces.



**Figure 6**. Statistical data on the critical rupture thickness of wetting films on a) octadecyltrichlorosilane-treated quartz plates and b) methyltrichlorosilane-treated quartz plates. C) Interference fringes of the wetting films formed on MTS-treated and OTS-treated hydrophobic quartz plates before and after the film rupture.

The silanization reaction creates a very strong hydrophobic surface on a quartz surface with an equilibrium water contact angle of 85° or above. Alternatively, cetyltrimethylammonium bromide (CTAB) may be used to hydrophobize the quartz plates in water. The cationic surfactant molecules adsorb on the freshly cleaned quartz plates, with the head polar group pointing towards the quartz plate, while the hydrocarbon tails pointing towards the aqueous phase.

Film stability was investigated by impacting an air bubble against a freshly cleaned quartz plate in  $10^{-4}$  M CTAB aqueous solutions. The water contact angles on the CTAB-adsorbed quartz surfaces were

approximately  $50^{\circ}$ . Figure 7a shows a spatiotemporal thickness profile of the TLFs on the quartz plates in  $10^{-4}$ M CTAB aqueous solutions. It takes 80 milliseconds (ms) after the initial impact for the TLF to drain and rupture on the CTAB-adsorbed quartz plates. The spatiotemporal thickness profile (Fig. 7b) revealed that the TLF ruptured at a critical rupture thickness of 550 nm in this scenario. Figure 7c shows the variability (or statistics) of critical rupture thickness on the quartz plates in  $10^{-4}$  M CATB solutions. The results showed that the critical rupture thicknesses of the TLFs were in the range of 350-550 nm, with a medium critical rupture thickness of 450 nm. Clearly, the critical rupture thickness ( $h_c$ ) of wetting films on weakly hydrophobic surfaces (50-70°) under a high Reynolds condition was much higher than those obtained under the quiescent condition. At this critical rupture thickness, the effect of disjoining pressure may be negligible since a typical effective range for the disjoining pressure was 0-200 nm. Beyond 200 nm, the effect of disjoining pressure may not be as significant as other factors.

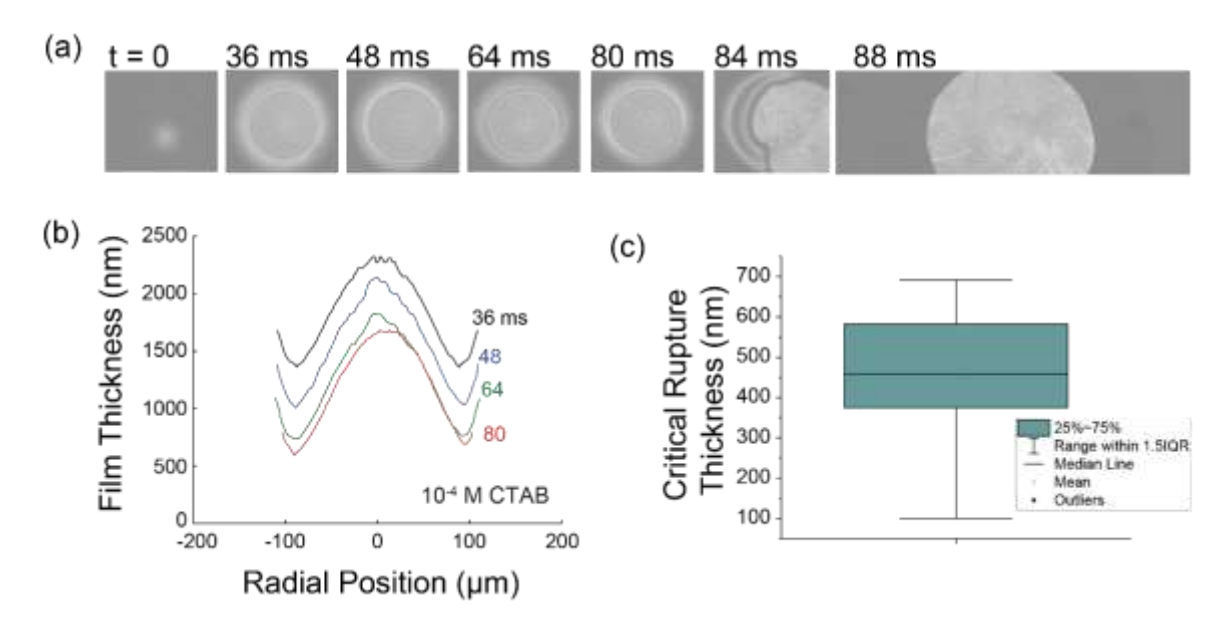


Figure 7. Dynamics and stability of the thin liquid films (TLFs) on the quartz plates in  $10^{-4}$  M cetyltrimethylammonium bromide (CTAB) aqueous solutions. a) timed series of interference fringes of thin liquid films between a free-rising air bubble and a quartz plate; b) spatiotemporal thickness profile of the TLFs; c) statistics on the critical rupture thickness of the wetting films formed on quartz plates in  $10^{-4}$  M CTAB aqueous solutions.

#### 3.4 Effect of Surfactant on Film Stability

In this work, the effect of 1-octanol concentration on the stability of thin liquid films on hydrophobized quartz plates was investigated. The quartz plates were hydrophobized in 10<sup>-3</sup> M OTS-in-toluene solution for 30 minutes. The equilibrium water contact angles on hydrophobized quartz plates were 90°. Figure 8 compares spatiotemporal thickness profiles of the representative TLFs between free-rising air bubbles and hydrophobic quartz surfaces at different 1-octanol concentrations. The wetting films of DI water on hydrophobic surfaces was highly unstable, and the film ruptured at a critical rupture thickness of 900 nm. The critical rupture thickness of the wetting films was decreased with increasing 1-octanol concentrations.

As shown, the critical rupture thickness of the wetting film was 400-700 nm in  $10^{-5}$  M 1-octanol aqueous solution. The critical rupture thicknesses of the wetting films were decreased to 200-400 nm in  $3x10^{-4}$  M 1-octanol aqueous solutions. Shortly after the wetting film reached its critical rupture thickness, the wetting film ruptured, followed by a spreading of a three-phase contact line (TPCL) on the hydrophobic surface.

Repetitive film stability experiments were performed at different concentrations of 1-octanol solutions. At least three different quartz plates were used in these experiments. Figure 9 compares the effect of 1-octanol concentration on a) critical lifetime and b) critical rupture thickness of the wetting films. The t=0 was defined as the moment when the air bubble first collides with the upper quartz plate. The critical rupture time was increased from 10-50 ms in water to 4-5 seconds in  $10^{-4}$  M and  $3x10^{-4}$  M 1-octanol solutions. Also shown in Figure 9 are the critical rupture thicknesses of the wetting films on OTS-treated hydrophobic surfaces at different 1-octanol concentrations. The medium critical rupture thickness of the wetting films was decreased from 900 nm in water to 400-500 nm in  $10^{-5}$  M 1-octanol solution and further down to 200-250 nm in  $3x10^{-4}$  M 1-octanol solution. At  $3x10^{-4}$  M 1-octanol solution, the surface tension of the liquid was also decreased to 65 mN/m due to the adsorption of 1-octanol at the air-water interface. The present result suggests that the presence of surfactant molecules in the aqueous solution extends the lifetime of the wetting films, resulting in more stable wetting films.

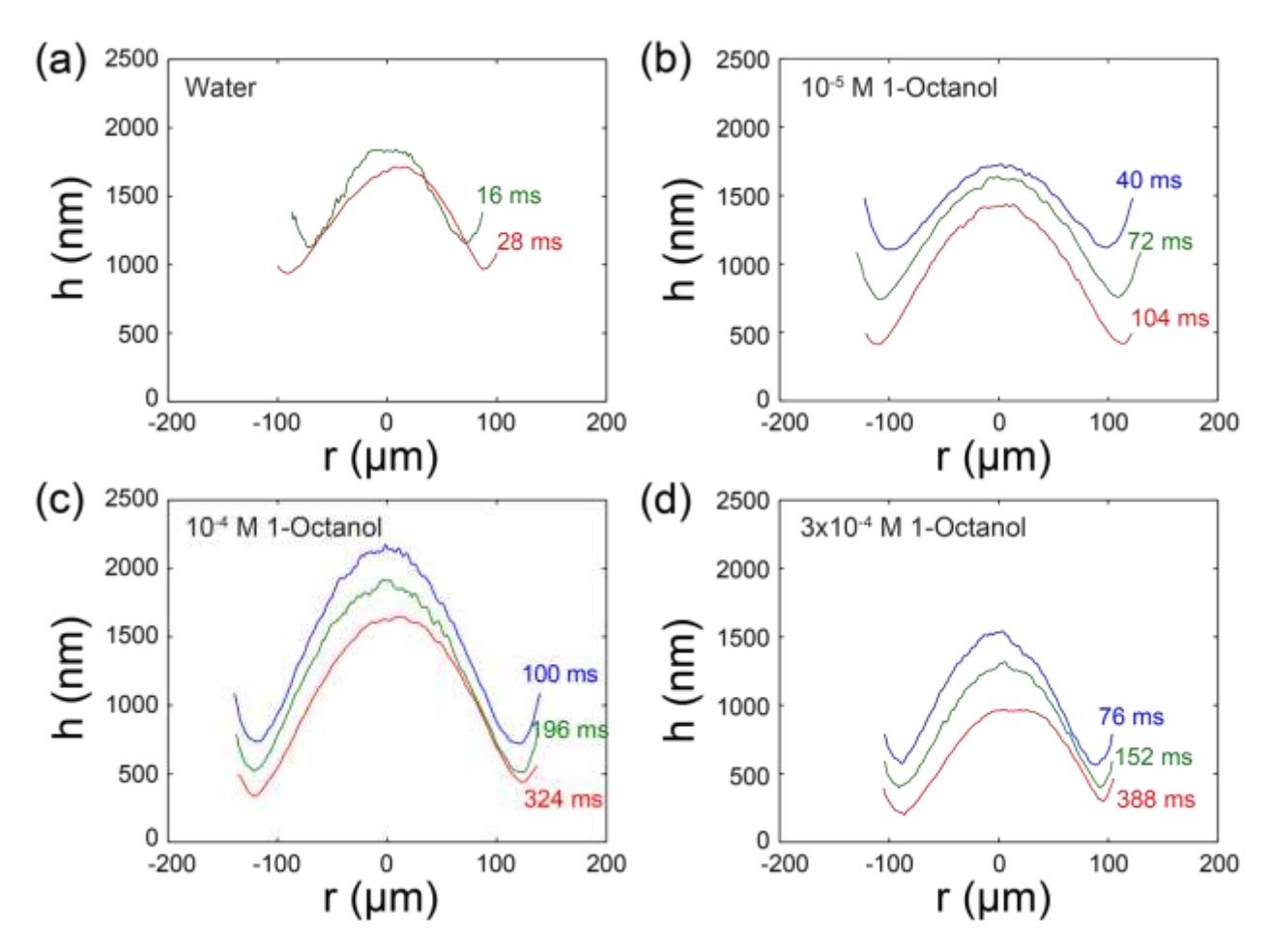


**Figure 8**. Spatial and temporal thickness profiles of the thin liquid film between free-rising air bubbles and hydrophobized quartz plates in a) water, b)  $10^{-5}$  M, c)  $10^{-4}$  M, and d)  $3x10^{-4}$  M 1-octanol aqueous solutions.

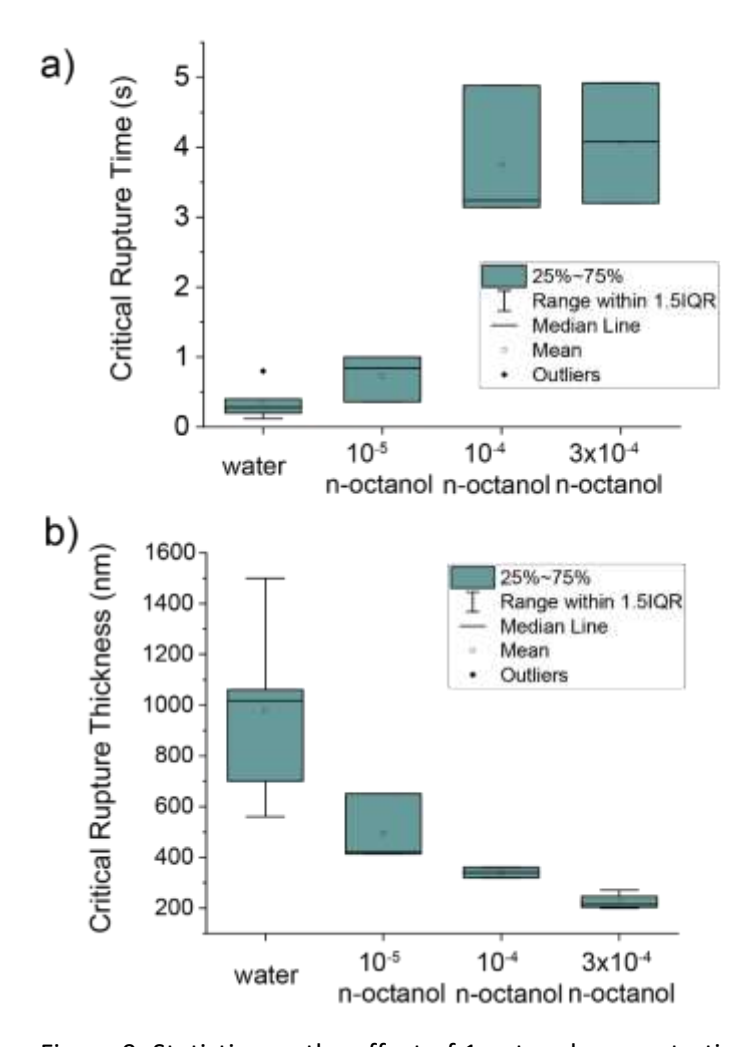


Figure 9. Statistics on the effect of 1-octanol concentration on both the critical rupture thickness of the thin liquid film (TLFs) during an impact of a free-rising air bubble and OTS-treated hydrophobic quartz plates. The effect of 1-octanol on the surface tension of the aqueous solutions as well as the water contact angles of the 1-octanol aqueous solution on hydrophobic OTS quartz plates.

#### 4. Discussion

As presented in the results above, the present work, for the first time, revealed the dynamics and stability of thin liquid films (TLFs) during the impact of a free-rising air bubble on hydrophobic surfaces. This work is a significant addition to the interferometric studies done a decade ago on the dynamics of a wetting film on a hydrophilic plate<sup>32</sup>. One of key challenges with an early investigation on unstable TLFs was that the film may rupture at 200 nm or above on hydrophobic surfaces. At this distance, the use of monochromatic interferometry technique even coupled with a high-speed photography system was unable to determine the exact order of the interference fringes at which the film was ruptured. The multi-wavelength synchronized reflection interferometry microscope (SRIM) technique resolves this challenge

by recording multiple interference fringes of the TLFs simultaneously at distinct wavelengths. By matching synchronized fringe patterns recorded at distinct wavelengths, one can determine fringe orders easily.

The present work demonstrated that the thin liquid films (TLFs) in water were highly unstable during the impact of a free-rising air bubble and a hydrophobic surface. The critical rupture thickness of the TLFs on very hydrophobic surfaces having water contact angles of 70-95° widely spread over the range of 400-2000 nm. On week hydrophobic surfaces having water contact angles of 40-60°, the critical rupture thicknesses were in the range of 200-600 nm. The present result is different from the previous results, which the stability of wetting films was investigated under a quasi-equilibrium condition<sup>13, 35</sup>. These experimental conditions were achieved by slowly bringing one surface against another<sup>11, 35</sup> or slowly withdrawing the liquid from thin liquid films (TLF)<sup>14</sup>. The Reynolds number was far below 1. Under these quasi-equilibrium conditions, the wetting film on hydrophobic surfaces typically ruptured at 0-200 nm, with a few exceptions in which the film ruptured at 200 nm or beyond. At this distance, the disjoining pressure can play a significant role in destabilizing the wetting films<sup>11, 13</sup>. In a comparison, during the impact of a free-rising air bubble on solid surfaces, the bubble's impact velocity was 100-2000 mm/s, depending on bubble sizes. After a few bounces off the surfaces, the impact velocity was significantly decreased. The TLF ruptures at 400 nm or beyond under the dynamic condition, which is more relevant to industrial froth flotation applications. At this distance, the disjoining pressure was negligible.

In the presence of surfactants in the aqueous solutions, with a capacity of reducing surface tension of the aqueous solutions, the wetting films were found to be more stable. The critical rupture thickness decreases with increasing the surfactant concentration. Correspondingly, the lifetime of the wetting film was increased significantly after increasing the surfactant concentration. The lifetime of the wetting films was increased from 8-40 milliseconds (ms) in DI water to 500-1000 milliseconds (ms) in  $3x10^{-4}$  M 1-octanol aqueous solutions.

Several theories have been proposed to explain the film rupture phenomena, including a) the presence of nanobubbles or other surface asperity on hydrophobic surfaces 16, 17, b) a propagation of the wave at the air/water interface19, c) attractive van der Walls, electrostatic double-layer, and hydrophobic disjoining pressures<sup>11, 13</sup>, and d) the gas channel<sup>18</sup>. For the nanobubble theory, the presence of pancake-shaped nanobubbles on the hydrophobic surfaces effectively reduces the effective distance between the macrosized air bubble and nano-sized air bubbles. The same principle applies to any surface asperity. As described earlier, the disjoining pressure is negligible at far above 200 nm. Figure 10 shows a possible mechanism for the film rupture between a free-rising air bubble and a hydrophobic solid surface under the high Reynolds condition. The gas channel theory was originally proposed by Yaminsky and Ninham<sup>36</sup>. The authors of this work believe that this theory matches well with the experimental data obtained in this work under the dynamic free-rising bubble conditions investigated in this work. The surface hydrophobicity of the solid surfaces induced film instability that resulted in the rupture of wetting films by forming a dissolved gas nucleus in the wetting films or by transporting gas molecules in the air bubble onto the hydrophobic surfaces. The more hydrophobic the solid surfaces are, the more likely the gas channel will be formed. The gas channel formation is very likely associated with the high impact velocity compared with those obtained in low impact velocity conditions. The formation of a cavity and/or gas channel is a random event, and therefore, the critical rupture thickness may vary significantly. The presence of surface-active molecules (surfactants) at the air/water interface can significantly reduce the chance for film rupture. The occupation of surfactant molecules at the air/water interface effectively increases the difficulty for air diffuse across the interface.

The authors of this work will not rule out other possible reasons for the film rupture, including waves or the presence of nanobubbles on the hydrophobic substrates. The presence of asperity, particularly these large-size asperities, will effectively reduce the effective separation distance between the air bubble and the solid surface without significantly impacting the repulsive hydrodynamic pressure. As a result, the effective rupture thickness was significantly reduced, resulting in an easy rupture of the wetting films.

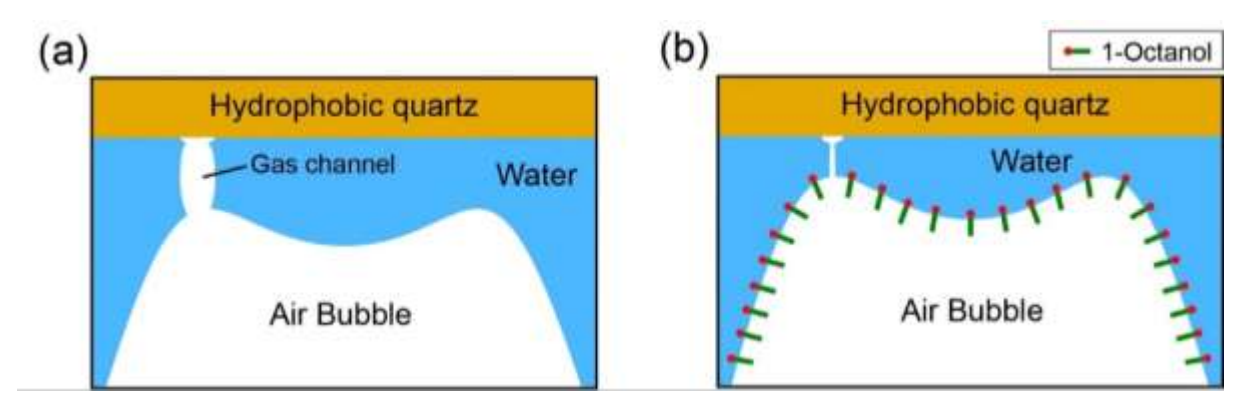


Figure 10. A possible mechanism in the rupture of the critical rupture thickness of wetting films on hydrophobic surfaces during an impact of a free-rising air bubble on hydrophobic quartz plates.

## 5. Conclusion and Summary

In this study, dynamics of thin liquid films (TLF) between free-rising air bubbles and hydrophobic quartz plates was investigated for the first time using a two-wavelength synchronized reflection interferometry microscope (SRIM). With this instrumentation, the spatiotemporal thickness profiles of the TLFs during the collision between free-rising air bubbles and stationary hydrophobic quartz plates were directly determined. The two-wavelength SRIM system allows an accurate film thickness measurement in the range of 0-2400 nm by taking advantage of distinct monochromatic fringe patterns captured at two wavelengths. The present study expanded the previous work on bubble-surface attachment from hydrophilic surfaces to hydrophobic surfaces. This is the first time that the critical rupture thicknesses of the TLF formed on hydrophobic surfaces under dynamic conditions were determined experimentally.

The results showed that the TLFs between free-rising air bubbles and hydrophobic surfaces ruptured at the closest separation distance of 200-1000 nm. This observed critical rupture thickness for the TLFs under a free rising condition was significantly larger than those obtained under a quasi-equilibrium condition. In addition, surface asperity was found to be an important factor in destabilizing the TLFs on hydrophobic surfaces. The polymerization of silane chemicals on the hydrophobic quartz plates resulted in a formation of micron-sized hydrophobic substances on the surfaces, facilitating the film rupture and shortening the lifetime of the wetting films. Furthermore, the presence of surfactant molecules at the air/water interfaces stabilized the TLFs, reduced the critical rupture thickness, and extended the lifetime of the wetting films.

Based on all results presented in this work, it is reasonable to assume that the film rupture under the impact of a free-rising air bubble against a flat surface was unlikely attributed to the presence of any types

of disjoining pressure. Instead, the rupture of the wetting films was likely due to a diffusion of gas molecules from air bubbles through the TLFs onto hydrophobic solid surfaces. The presence of surfactants at the air-water interface significantly reduced the diffusion of gas molecules across the interface, thus preventing the film from rupturing. The present results provide direct experimental evidence for the short lifetime of the thin liquid film (TLF) during a bubble's impact on very hydrophobic surfaces.

## 6. Acknowledgement

The authors would like to acknowledge the financial support from the National Science Foundation (NSF). The award number is 1920013.

## 7. References

- (1) Ralston, J. Thin films and froth flotation. *Advances in Colloid and Interface Science* **1983**, *19* (1), 1-26. DOI: https://doi.org/10.1016/0001-8686(83)80002-5.
- (2) Gao, Y.; Pan, L. Understanding the mechanism of froth flotation of molybdenite using oily collectors from a perspective of thinning and rupture of thin liquid film. *Minerals Engineering* **2021**, *163*, 106805.
- (3) Xing, Y.; Gui, X.; Pan, L.; Pinchasik, B.-E.; Cao, Y.; Liu, J.; Kappl, M.; Butt, H.-J. Recent experimental advances for understanding bubble-particle attachment in flotation. *Advances in colloid and interface science* **2017**, *246*, 105-132.
- (4) Wang, L.; Yoon, R.-H. Hydrophobic Forces in the Foam Films Stabilized by Sodium Dodecyl Sulfate: Effect of Electrolyte. *Langmuir* **2004**, *20* (26), 11457-11464. DOI: 10.1021/la048672g.
- (5) Tchoukov, P.; Yang, F.; Xu, Z.; Dabros, T.; Czarnecki, J.; Sjoblom, J. Role of asphaltenes in stabilizing thin liquid emulsion films. *Langmuir* **2014**, *30* (11), 3024-3033.
- (6) Czarnecki, J.; Khristov, K.; Masliyah, J.; Panchev, N.; Taylor, S. D.; Tchoukov, P. Application of Scheludko–Exerowa thin liquid film technique to studies of petroleum W/O emulsions. *Colloids and Surfaces A: Physicochemical and Engineering Aspects* **2017**, *519*, 2-10. DOI: <a href="https://doi.org/10.1016/j.colsurfa.2016.04.040">https://doi.org/10.1016/j.colsurfa.2016.04.040</a>.
- (7) Israelachvili, J.; Min, Y.; Akbulut, M.; Alig, A.; Carver, G.; Greene, W.; Kristiansen, K.; Meyer, E.; Pesika, N.; Rosenberg, K. Recent advances in the surface forces apparatus (SFA) technique. *Reports on Progress in Physics* **2010**, *73* (3), 036601.
- (8) Kappl, M.; Butt, H. J. The colloidal probe technique and its application to adhesion force measurements. *Particle & Particle Systems Characterization: Measurement and Description of Particle Properties and Behavior in Powders and Other Disperse Systems* **2002**, *19* (3), 129-143.
- (9) Sheludko, A. Thin liquid films. Advances in Colloid and Interface Science 1967, 1 (4), 391-464.
- (10) Huang, K.; Yoon, R.-H. Surface forces in the thin liquid films (TLFs) of water confined between nalkane drops and hydrophobic gold surfaces. *Langmuir* **2019**, *35* (48), 15681-15691.
- (11) Pan, L.; Yoon, R.-H. Measurement of hydrophobic forces in thin liquid films of water between bubbles and xanthate-treated gold surfaces. *Minerals Engineering* **2016**, *98*, 240-250.
- (12) Wang, L.; Yoon, R.-H. Role of hydrophobic force in the thinning of foam films containing a nonionic surfactant. *Colloids and Surfaces A: Physicochemical and Engineering Aspects* **2006**, *282*, 84-91.
- (13) Huang, K.; Yoon, R.-H. Control of bubble  $\zeta$ -potentials to improve the kinetics of bubble-particle interactions. *Minerals Engineering* **2020**, *151*, 106295.
- (14) Pan, L.; Jung, S.; Yoon, R.-H. Effect of hydrophobicity on the stability of the wetting films of water formed on gold surfaces. *Journal of colloid and interface science* **2011**, *361* (1), 321-330.

- (15) Manev, E. D.; Nguyen, A. V. Critical thickness of microscopic thin liquid films. *Advances in Colloid and Interface Science* **2005**, *114-115*, 133-146. DOI: <a href="https://doi.org/10.1016/j.cis.2004.07.013">https://doi.org/10.1016/j.cis.2004.07.013</a>.
- (16) Schulze, H. J.; Stöckelhuber, K. W.; Wenger, A. The influence of acting forces on the rupture mechanism of wetting films nucleation or capillary waves. *Colloids and Surfaces A: Physicochemical and Engineering Aspects* **2001**, *192* (1), 61-72. DOI: https://doi.org/10.1016/S0927-7757(01)00717-8.
- (17) Slavchov, R.; Radoev, B.; Stöckelhuber, K. W. Equilibrium profile and rupture of wetting film on heterogeneous substrates. *Colloids and Surfaces A: Physicochemical and Engineering Aspects* **2005**, *261* (1), 135-140. DOI: <a href="https://doi.org/10.1016/j.colsurfa.2004.12.031">https://doi.org/10.1016/j.colsurfa.2004.12.031</a>.
- (18) Christenson, H. K.; Claesson, P. M. Cavitation and the interaction between macroscopic hydrophobic surfaces. *Science* **1988**, *239* (4838), 390-392.
- (19) Ivanov, I.; Radoev, B.; Manev, E.; Scheludko, A. Theory of the critical thickness of rupture of thin liquid films. *Transactions of the Faraday Society* **1970**, *66*, 1262-1273.
- (20) Kosior, D.; Zawala, J.; Malysa, K. Influence of n-octanol on the bubble impact velocity, bouncing and the three phase contact formation at hydrophobic solid surfaces. *Colloids and Surfaces A: Physicochemical and Engineering Aspects* **2014**, *441*, 788-795.
- (21) Christenson, H. K.; Yaminsky, V. Is the long-range hydrophobic attraction related to the mobility of hydrophobic surface groups? *Colloids and Surfaces A: Physicochemical and Engineering Aspects* **1997**, 129, 67-74.
- (22) Pan, L.; Yoon, R.-H. Effects of elctrolytes on the stability of wetting films: Implications on seawater flotation. *Minerals Engineering* **2018**, *122*, 1-9.
- (23) Christenson, H. K.; Fang, J.; Ninham, B. W.; Parker, J. L. Effect of divalent electrolyte on the hydrophobic attraction. *Journal of Physical Chemistry* **1990**, *94* (21), 8004-8006.
- (24) Wang, J.; Yoon, R.-H.; Eriksson, J. C. Excess thermodynamic properties of thin water films confined between hydrophobized gold surfaces. *Journal of colloid and interface science* **2011**, *364* (1), 257-263.
- (25) Krasowska, M.; Zawala, J.; Malysa, K. Air at hydrophobic surfaces and kinetics of three phase contact formation. *Advances in Colloid and Interface Science* **2009**, *147-148*, 155-169. DOI: <a href="https://doi.org/10.1016/j.cis.2008.10.003">https://doi.org/10.1016/j.cis.2008.10.003</a>.
- (26) Krasowska, M.; Malysa, K. Wetting films in attachment of the colliding bubble. *Advances in colloid and interface science* **2007**, *134*, 138-150.
- (27) Zawala, J.; Krasowska, M.; Dabros, T.; Malysa, K. Influence of bubble kinetic energy on its bouncing during collisions with various interfaces. *The Canadian Journal of Chemical Engineering* **2007**, *85* (5), 669-678.
- (28) Niecikowska, A.; Krasowska, M.; Ralston, J.; Malysa, K. Role of surface charge and hydrophobicity in the three-phase contact formation and wetting film stability under dynamic conditions. *The Journal of Physical Chemistry C* **2012**, *116* (4), 3071-3078.
- (29) Krasowska, M.; Malysa, K. Kinetics of bubble collision and attachment to hydrophobic solids: I. Effect of surface roughness. *International Journal of Mineral Processing* **2007**, *81* (4), 205-216. DOI: <a href="https://doi.org/10.1016/j.minpro.2006.05.003">https://doi.org/10.1016/j.minpro.2006.05.003</a>.
- (30) Vakarelski, I. U.; Langley, K. R.; Yang, F.; Thoroddsen, S. T. Interferometry and Simulation of the Thin Liquid Film between a Free-Rising Bubble and a Glass Substrate. *Langmuir* **2022**, *38* (7), 2363-2371. DOI: 10.1021/acs.langmuir.1c03374.
- (31) Hendrix, M. H. W.; Manica, R.; Klaseboer, E.; Chan, D. Y. C.; Ohl, C.-D. Spatiotemporal Evolution of Thin Liquid Films during Impact of Water Bubbles on Glass on a Micrometer to Nanometer Scale. *Physical Review Letters* **2012**, *108* (24), 247803. DOI: 10.1103/PhysRevLett.108.247803.
- (32) Parkinson, L.; Ralston, J. The Interaction between a Very Small Rising Bubble and a Hydrophilic Titania Surface. *The Journal of Physical Chemistry C* **2010**, *114* (5), 2273-2281. DOI: 10.1021/jp9099754.

- (33) Manica, R.; Parkinson, L.; Ralston, J.; Chan, D. Y. C. Interpreting the Dynamic Interaction between a Very Small Rising Bubble and a Hydrophilic Titania Surface. *The Journal of Physical Chemistry C* **2010**, *114* (4), 1942-1946. DOI: 10.1021/jp911104b.
- (34) Pan, L.; Jung, S.; Yoon, R.-H. A fundamental study on the role of collector in the kinetics of bubble–particle interaction. *International journal of mineral processing* **2012**, *106*, 37-41.
- (35) Huang, K.; Yoon, R.-H. Effect of  $\zeta$ -potentials on bubble-particle interactions. *Mining, Metallurgy & Exploration* **2019**, *36*, 21-34.
- (36) Yaminsky, V. V.; Ninham, B. W. Hydrophobic force: Lateral enhancement of subcritical fluctuations. *Langmuir* **1993**, *9* (12), 3618-3624.